

Parameter-Free Effective Potential Method for Use in Particle-Based Device Simulations

S. Ahmed¹, C. Ringhofer² and D. Vasileska¹

¹*Department of Electrical Engineering, Arizona State University, Tempe, AZ, 85287-5706*

²*Department of Mathematics, Arizona State University, Tempe, AZ 85287*

E-mail: sahmed@asu.edu, ringhofer@asu.edu, vasileska@asu.edu

Abstract

We propose a novel *parameter-free* effective potential scheme for use in conjunction with particle-based simulations. The method is based on a perturbation theory around thermodynamic equilibrium and leads to an effective potential scheme in which the size of the electron depends upon its energy. The approach has been tested on the example of a MOS-capacitor by retrieving the correct sheet electron density. It has also been used in simulations of a 25 nm *n*-channel nano-MOSFET that requires very high substrate doping to prevent the punch-through effect which, on the other hand, leads to pronounced quantum mechanical space-quantization effects. We find that the use of the new effective potential approach gives correct experimentally verified threshold voltage shifts of about 220 mV and drain current degradation of about 30%. The largest contribution comes from the barrier field which is pre-computed in the initial stages of the simulation. Thus, rough estimates on the role of quantum effects on device operation can be made by using the barrier field only.

1. The Evolution of the Idea for Use of Effective Potentials

The inclusion of one-particle quantum effects in the description of the inversion layer at the semiconductor/oxide interface of a metal-oxide-semiconductor device involves solving the 1D Schrödinger equation for the carriers in an approximately triangular potential well self-consistently with a 1D Poisson equation. As a result, one obtains bound states which give rise to two major features: *reduced sheet density* and *charge set-back*. Namely, since the lowest bound state can be regarded as the new bottom of the conduction band, the spacing between the Fermi level and the conduction band edge is effectively increased, which results in the reduced sheet charge density with respect to the case in which quantum effects are excluded. Moreover, the probability density in the lowest bound state now has a maximum away from the semiconductor/oxide interface, resulting in charge displacement from the oxide, which accounts for an effective increase in the oxide thickness.

An alternative to solving the Schrödinger wave equation is the use of quantum potentials. The idea of quantum potentials originates from the hydrodynamic formulation of quantum mechanics, first introduced by de Broglie and Madelung [1,2,3], and later developed by Bohm [4,5]. In this picture, the wave function is written in complex form in terms of its amplitude $R(\mathbf{r},t)$ (the density function) and phase $S(\mathbf{r},t)$, $\psi(\mathbf{r},t) = R(\mathbf{r},t)\exp[iS(\mathbf{r},t)/\hbar]$. These are then substituted back into the Schrödinger equation to obtain the following coupled equations of motion for the density and phase

$$\frac{\partial \rho(\mathbf{r},t)}{\partial t} + \nabla \cdot \left(\rho(\mathbf{r},t) \frac{1}{m} \nabla S(\mathbf{r},t) \right) = 0, \quad (1)$$

$$-\frac{\partial S(\mathbf{r},t)}{\partial t} = \frac{1}{2m} [\nabla S(\mathbf{r},t)]^2 + V(\mathbf{r},t) + V_Q(\rho, \mathbf{r}, t), \quad (2)$$

where $\rho(\mathbf{r}, t) = R(\mathbf{r}, t)^2$ is the probability density. By identifying the velocity as $\mathbf{v} = \nabla S / m$, and the flux as $\mathbf{j} = \rho \mathbf{v}$, equation (1) becomes the continuity equation. Hence, equations (1) and (2) arising from this so-called *Madelung transformation* to the Schrödinger equation have the form of classical hydrodynamic equations with the addition of an extra potential, often referred to as the *quantum* or *Bohm potential*, written as

$$V_Q = -\frac{\hbar^2}{2mR} \nabla^2 R \rightarrow -\frac{\hbar^2}{2m\sqrt{n}} \nabla^2 \sqrt{n} \quad (3)$$

where the density n , is related to the probability density as $n(\mathbf{r}, t) = N\rho(\mathbf{r}, t) = NR(\mathbf{r}, t)^2$, where N is the total number of particles. The Bohm potential essentially represents a field through which the particle interacts with itself. It has been used, for example, in the study of wave packet tunneling through barriers [6], where the effect of the quantum potential is shown to lower or smoothen barriers, and hence *allow* for the particles to leak through.

An alternate form of the quantum potential was proposed by Iafrate, Grubin and Ferry [7], who derived a form of the quantum potential based on moments of the *Wigner-Boltzmann equation*, the kinetic equation describing the time evolution of the Wigner distribution function [8]. Their form, based on moments of the Wigner function in the pure state, and involving an expansion of order $O(\hbar^2)$, is given by

$$V_Q = -\frac{\hbar^2}{8m} \nabla^2 (\ln n), \quad (4)$$

which is sometimes referred to as the *Wigner potential*, or as the density gradient correction. Such quantum potentials have been extensively used in *density-gradient* and *quantum-hydrodynamic* methods. Their use in particle-based simulation schemes becomes questionable

due to the presence of statistical noise in the representation of the electron density and the considerable difficulty to calculate the second derivative of the density on a completely unstructured mesh given by the particle discretization.

To avoid this problem, Ferry and Zhou derived a form for a smooth quantum potential [9], based on the effective classical partition function of Feynman and Kleinert [10]. More recently, Gardner and Ringhofer [11] derived a smooth quantum potential for hydrodynamic modeling, valid to all orders of \hbar^2 , which involves a smoothing integration of the classical potential over space and temperature. There, it was shown that, close to the equilibrium regime, the influence of the potential on the ensemble can be replaced by the classical influence of a smoothed non-local barrier potential. While this effective potential depends non-locally on the density, it does not directly depend on its derivatives. Through this effective quantum potential, the influence of the barriers on an electron is felt at quite some distance from the barrier. The smoothed effective quantum potential has been used successfully in quantum-hydrodynamic simulations of resonant tunneling effects in one dimensional double-barrier structures [12].

In analogy to the smoothed potential representations discussed above for the quantum hydrodynamic models, it is desirable to define a smooth quantum potential for use in quantum particle-based simulations. Ferry suggested an *effective potential scheme* that emerges from a wave packet description of the particle motion, where the extent of the wave packet spread is obtained from the range of wavevectors in the thermal distribution function (characterized by an electron temperature). The effective potential, V_{eff} , is related to the self-consistent Hartree potential, V , obtained from the Poisson equation, through an integral smoothing relation

$$V_{\text{eff}}(\mathbf{x}) = \int V(\mathbf{x} + \mathbf{y}) G(\mathbf{y}, a_0) d\mathbf{y}, \quad (5)$$

where G is a Gaussian with standard deviation a_0 . This effective potential V_{eff} is then used to calculate the electric field that accelerates the carriers in the transport kernel of our in-house Monte Carlo particle-based device simulator. The calculation of V_{eff} has a fairly low computational cost, but the requirement that the electric field is updated every 0.01 fs to get physically accurate particle trajectories and to eliminate the artificial heating of the carriers in the vicinity of the Si/SiO₂ interface (where the fields are the strongest), adds to the computational cost. Note also that *within this approach the parameter a_0 has to be adjusted in the initial stages of the simulation* via comparisons of the sheet/line density of the Q2D/Q1D structure being investigated using the effective potential approach and the 1D/2D Schrödinger-Poisson simulations.

2. Thermodynamic Effective Quantum Potential

The basic idea of the thermodynamic approach to effective quantum potentials is that the resulting semiclassical transport picture should yield the correct thermalized equilibrium quantum state. Using quantum potentials, one generally replaces the quantum Liouville equation

$$\partial_t \rho + \frac{i}{\hbar} [H, \rho] = 0 \quad (6)$$

for the density matrix $\rho(x, y)$ by the classical Liouville equation

$$\partial_t f + \frac{\hbar}{2m^*} k \cdot \nabla_x f - \frac{1}{\hbar} \nabla_x V \cdot \nabla_k f = 0, \quad (7)$$

for the classical density function $f(x, k)$. Here, the relation between the density matrix and the density function f is given by the Weyl quantization

$$f(x, k) = W[\rho] = \int \rho(x + y/2, x - y/2) \exp(ik \cdot y) dy. \quad (8)$$

The thermal equilibrium density matrix in the quantum mechanical setting is given by $\rho^{eq} = e^{-\beta H}$, where $\beta = 1/k_B T$ is the inverse energy, and the exponential is understood as a matrix exponential, i.e. $\rho^{eq}(x, y) = \sum_{\lambda} \psi_{\lambda}(x) \exp(-\beta \lambda) \psi_{\lambda}(y)^*$ holds, with $\{\psi_{\lambda}\}$ the orthonormal eigensystem of the Hamiltonian H . In the semiclassical transport picture, on the other hand, the thermodynamic equilibrium density function f_{eq} is given by the Maxwellian

$$f_{eq}(x, k) = \exp\left(-\frac{\beta \hbar^2 |k|^2}{2m^*} - \beta V\right). \text{ Consequently, to obtain the quantum mechanically correct}$$

equilibrium states in the semiclassical Liouville equation with the effective quantum potential V^Q , we set

$$f_{eq}(x, k) = \exp\left(-\frac{\beta \hbar^2 |k|^2}{2m^*} - \beta V^Q\right) = W[\rho^{eq}] = \int \rho(x + y/2, x - y/2) \exp(ik \cdot y) dy. \quad (9)$$

This basic concept was originally introduced by Feynman and Kleinert [10]. Different forms of the effective quantum potential arise from different approaches to approximate the matrix exponential $e^{-\beta H}$.

In the approach presented in this paper, we represent $e^{-\beta H}$ as the Green's function of the semigroup generated by the exponential. Introducing an artificial dimensionless parameter γ and defining $\rho(x, y, \gamma) = \sum_{\lambda} \psi_{\lambda}(x) \exp(-\gamma \beta \lambda) \psi_{\lambda}(y)^*$, we obtain a heat equation for ρ by differentiating ρ with respect to γ and using the eigenfunction property of the wave functions ψ_{λ} .

This heat equation is referred to as the Bloch equation

$$\partial_\gamma \rho = -\frac{\beta}{2}(H \cdot \rho + \rho \cdot H), \quad \rho(x, y, \gamma=0) = \delta(x-y), \quad (10)$$

and $\rho^{eq}(x, y)$ is given by $\rho^{eq}(x, y, \gamma=1)$. Under the Weyl quantization this becomes, with the

usual Hamiltonian $H = -\frac{\hbar^2}{2m^*}\Delta_x + V$ and defining the effective energy E by $f = W[\rho] = e^{-\beta E}$,

$$\begin{aligned} \partial_\gamma E &= \frac{\beta \hbar^2}{8m^*} \left(\Delta_x E - \beta |\nabla_x E|^2 \right) + \frac{\hbar^2 |k|^2}{2m^*} + \\ &\frac{1}{2(2\pi)^3} \sum_{\nu=\pm 1} \int V(x+\nu y/2) \exp \left[\beta E(x, k, \gamma) - \beta E(x, q, \gamma) + iy(k-q) \right] dq dy, \quad (11) \\ E(x, k, \gamma=0) &= 0. \end{aligned}$$

The effective quantum potential is in this formulation given by $E(x, k, \gamma=1) = V_Q + \frac{\hbar^2 |k|^2}{2m^*}$. The

logarithmic Bloch equation is now solved ‘asymptotically’, using the *Born approximation*, i.e. by iteratively inverting the highest order differential operator (the Laplacian). This involves successive solution of a heat equation for which the Green’s function is well known, giving (see Ref. [13] for the details)

$$V^Q(x, k) = \frac{1}{(2\pi)^3} \int \frac{2m^*}{\beta \hbar^2 k \cdot \xi} \sinh \left(\frac{\beta \hbar^2 k \cdot \xi}{2m^*} \right) \exp \left(-\frac{\beta \hbar^2}{8m^*} |\xi|^2 \right) V(y) e^{i\xi \cdot (x-y)} dy d\xi. \quad (12)$$

Note that the effective quantum potential V^Q now depends on the wave vector k . For electrons at rest, i.e. for $k=0$, the effective potential V^Q reduces to the Gaussian smoothing given in Eq. (5).

Also note that *there are no fitting parameters in this approach*, i.e. the size of the wavepacket is determined by the particle’s energy.

The potential $V(y)$ that appears in the integral of Eq. (12) can be represented as a sum of two potentials: the barrier potential $V_B(x)$, which takes into account the discontinuity at the

Si/SiO₂ interface due to the difference in the semiconductor and the oxide affinities, and the Hartree potential $V_H(x)$ that results from the solution of the Poisson equation. Note that the barrier potential is 1D and independent of time and needs to be computed only once in the initialization stage of the code. On the other hand, the Hartree potential is 2D and time-dependent as it describes the evolution of charge from quasi-equilibrium to a non-equilibrium state. Since the evaluation of the effective Hartree potential, as given by Eq. (12), is very time consuming and CPU intensive, approximate solution methods have been pursued to resolve this term within a certain level of error tolerance.

We recall from the above discussion that the barrier potential is just a step-function. Under these circumstances $e\nabla_x V_B(x) = B(1,0,0)^T \delta(x_1)$, where B is the barrier height (on the order of 3.2 eV) and x_1 is a vector perpendicular to the interface. We actually need only the gradient of the potential so that, using the pseudo-differential operators (see Appendix A), we compute

$$\nabla_x V_B^Q(x, p) = \exp\left[\frac{\beta\hbar^2 |\nabla_x|^2}{8m^*}\right] \frac{2m^* \sin\left(\frac{\beta\hbar p \cdot \nabla_x}{2m^*}\right)}{\beta\hbar p \cdot \nabla_x} \nabla_x V_B(x). \quad (13)$$

This gives

$$e\nabla_x V_B^Q(x, p) = \frac{B}{2\pi} (1,0,0)^T \int \exp\left[-\beta \frac{\hbar^2 |\xi_1|^2}{8m^*}\right] \frac{2m^* \sinh\left(\frac{\beta\hbar p_1 \cdot \xi_1}{2m^*}\right)}{\beta\hbar p_1 \cdot \xi_1} e^{i\xi_1 \cdot x_1} d\xi_1. \quad (14)$$

Note that V_B^Q is only a function of (x_1, p_1) , i.e. it remains to be strictly one-dimensional, where x_1 and p_1 are the position and the momentum vector perpendicular to the interface. This, when combined with the fact that we have to calculate this integral only once, is a reason why we have

decided to tabulate the result given by Eq. (14) on a mesh. In Figure 1, we show the barrier field for low-energy (top panel) and for high-energy (bottom panel) electrons. In both cases we observe that the field decays almost exponentially with depth and increases with increasing the energy of the carriers. This is more clearly seen in the low-energy portion of the results given in Figure 1, where there is almost zero-field for low-energy electrons and a significant increase in the field for high-energy electrons.

The Hartree potential, as computed by solving the d -dimensional Poisson equation, depends in general upon d particle coordinates. For example, on a rectangular mesh the 2D Hartree potential is given by $V_H(x_1, x_2, t)$, and one has to evaluate $V_H^O(x_1, x_2, p_1, p_2, t)$ using Eq. (12) N times each time step for all particles position and momenta: $x^n, p^n, n = 1, \dots, N$ (where N is the number of electrons, which is large). This is, of course, an impossible task to be accomplished in finite time on present state-of-the-art computers. We, therefore, suggest the following scheme. According to (12), we evaluate the quantum potential by multiplying the Hartree potential by a function of $\hbar \nabla_x$, or by multiplying the Fourier transform of the Hartree potential by a function of $\hbar \xi$. We factor the expression in Eq. (12) into

$$V_H^O(x, k) = \frac{2im^*}{\beta \hbar^2 k \cdot \nabla_x} \sinh\left(\frac{\beta \hbar^2 k \cdot \nabla_x}{2im^*}\right) \exp\left(\frac{\beta \hbar^2}{8m^*} |\nabla_x|^2\right) V_H(x) = \frac{2im^*}{\beta \hbar^2 k \cdot \nabla_x} \sinh\left(\frac{\beta \hbar^2 k \cdot \nabla_x}{2im^*}\right) V_H^0(x), \quad (15)$$

with

$$V_H^0(x) = \exp\left(\frac{\beta \hbar^2}{8m^*} |\nabla_x|^2\right) V_H(x). \quad (16)$$

The evaluation of the potential $V_H^0(x)$, which is a version of the Gaussian smoothed potential due to Ferry [9], is computationally inexpensive since it does not depend on the wavevector k .

On the other hand, because of the Gaussian smoothing, $V_H^0(x)$ will be a smooth function of position, even if the Hartree potential $V_H(x)$ is computed via the Poisson equation where the electron density is given by a particle discretization. Therefore, the Fourier transform of the potential $V_H^0(x)$ will decay rapidly as a function of ξ , and it is admissible to use a Taylor expansion for small values of $h\xi$ in the rest of the operator. This gives

$$\frac{2im^*}{\beta h^2 k \cdot \nabla_x} \sinh\left(\frac{\beta h^2 k \cdot \nabla_x}{2im^*}\right) \approx 1 - \frac{\beta^2 h^4 (k \cdot \nabla_x)^2}{24(m^*)^2}, \quad (17)$$

or

$$\partial_{x_r} V_H^0(x^n, p^n) = \partial_{x_r} V_H^0(x^n) - \frac{\beta^2 h^2}{24m^{*2}} \sum_{j,k=1}^2 p_j^n p_k^n \partial_{x_j} \partial_{x_k} \partial_{x_r} V_H^0(x^n), \quad n=1, K, N \quad (18)$$

for all particles. This is done simply by numerical differentiation of the sufficiently smooth grid function V_H^0 and interpolation. The evaluation of (18) is the price we have to pay when we compare the computational cost of this approach as opposed to the Ferry approach [9] which uses simple forward, backward or centered difference scheme for the calculation of the electric field. However, *with this novel effective potential approach we avoid the use of adjustable parameters.*

3. Simulation Results

To verify the validity of our approach, we first performed self-consistent simulations of MOS capacitor structures and calculated the reduction in the sheet electron density due to the band-gap widening effect and the increase in the average distance of the carriers from the

interface proper. The simulation results from these investigations are shown in Figure 2. For the purpose of completeness, we also simulate this structure using SCHRED, the 1D Schrödinger-Poisson solver that was developed at Arizona State University and extended at Purdue University to include the capability of modeling double-gate structures. Notice the excellent agreement between the SCHRED simulation data for the sheet electron density and the simulation results obtained by utilizing the novel effective potential approach proposed in this paper.

Having performed these initial calibration tests and having been convinced that the method correctly predicts quantum effects in triangular potential wells, we proceed with the simulation of 25 nm MOSFET device. The parameters of the device structure being simulated are as follows: the substrate doping equals 10^{19} cm^{-3} , the doping of the source and drain regions is 10^{19} cm^{-3} , the junction extension is 30 nm, the oxide thickness is 1.2 nm and the gates are assumed to be metal gates with work-function equal to the semiconductor affinity. We have used relatively low doping of the source/drain regions to reduce the number of particles in the simulation ensemble (i.e. reduce the simulation time for computing one bias point). With comparison to Silvaco ATLAS simulations, we find that one order of magnitude smaller doping in the source/drain regions gives rise to significant series resistance effects which, in turn, leads to on-current degradation of about 20%. However, our choice for the source/drain doping is not going to affect the conclusions derived from this work.

First, in Figure 3, we show the carrier confinement within the triangular potential well with and without the inclusion of the quantum-mechanical size-quantization effects. From the results shown in this figure, it is evident that both the low-energy and the high-energy electrons are displaced by almost the same amount. Also note that there is practically no carrier heating for the case when the effective potential is used in calculating the driving electric field. The carrier

displacement from the interface proper is also seen from the results presented in Figure 4. Notice that there is approximately 2 nm shift of the electron density distribution near the source end of the channel when quantization effects are included in the model. Also note that carriers behave more like bulk carriers at the drain end of the channel and are displaced in the same manner when using both the classical and the quantum-mechanical model.

The channel length variation of the sheet electron density is shown in Figure 5. We use classical, fully-quantum $(V_H^Q + V_B^Q)$ and quantum-barrier field model (V_B^Q) for these calculations. We also compare our simulation results for the sheet electron density with those that utilize the approach due to Ferry. There are several noteworthy features to be observed on these figures. First, the pinch-off of the sheet electron density near the drain end of the channel is evident in all models used. Second, the barrier and the full-effective potential scheme give almost the same value for the sheet electron density, which suggests that the repulsive barrier field dominates over the attractive field due to the Hartree potential. Third, the method due to Ferry leads to significantly lower value for the sheet electron density, thus underestimating the drive current.

The average electron velocity and the average electron energy are shown in the left and the right panels of Figure 6, respectively. Comparing the results for the average carrier energy on the right panel, we see that the data for the case when we have not included the effective potential and the case when we have used the new model for the effective potential agree very well with each other. The approach due to Ferry gives significantly lower value for the carrier energy near the source end of the channel which has been explained to be due to the bandgap widening effect. When we confront these data with the results for the average electron velocity, we see that in the low-energy region near the source end of the channel the velocity is almost the

same for all cases considered. At the drain end, we find degradation of the velocity due to the smearing introduced by the quantum potential. Again, the inclusion of the barrier field and of the quantum-corrected Hartree term give similar values, which suggests that for the device being considered in this study only the barrier field has significant impact.

The device transfer and output characteristics are shown in Figure 7 and 8, respectively. Again, from both figures we see that the proposed full quantum potential and the barrier potential give similar values for the current. Looking more in detail the device transfer characteristics we find that the quantization effects lead to threshold voltage increase of about 220 mV. When properly adjusted for the oxide thickness difference, this result is consistent with previously published data. Evidently, the shift in the threshold voltage leads to a decrease in the on-state current by 30 %. The later observation confirms earlier findings that one must include quantum effects into the theoretical model to be able to properly predict the device threshold voltage and its on-state current.

4. Conclusions

In summary, a novel effective potential approach has been proposed and tested in simulations of quantization effects in 25 nm nano-MOSFET device. The approach is parameter free as the size of the electron depends upon its energy. We have justified the correctness of the approach with simulations of the gate voltage dependence of the sheet electron density and the average distance from the interface that were compared to equivalent SCHRED simulation results. The excellent agreement between these two data sets suggests that we are able to correctly predict the effective oxide thickness increase due to quantum-mechanical size-quantization effects that lead to a reduction of the sheet electron density. The nano-MOSFET

simulation results also confirm this charge displacement effect near the source end of the channel where quantization effects play significant role. Due to the larger smearing of the potential for high energy electrons, we see a decrease in the carrier velocity when quantization effects are included in the model. This leads to smaller drain current in both the device transfer and output characteristics. The charge displacement from the interface, and the effective increase of the oxide thickness, gives rise to a threshold voltage shift of ~ 220 mV which is consistent with earlier observations. The shift in the threshold voltage leads, in turn, to a drain current degradation of about 30 %. Hence, the observations presented here, that utilize the new effective potential approach, confirm that quantum-mechanical space-quantization effects must be included in the theoretical model to correctly predict the device behavior. In some cases, this can be achieved with the incorporation of the barrier field that is pre-computed in the initial stages of the simulation and does not require additional CPU time during the simulation sequence. We believe that *this new effective potential approach is more reliable in simulation of quantization effects in nano-scale devices with barriers that have different size and shape.*

Acknowledgements

The financial support from the Office of Naval Research under Contract No. N00014-99-1-03-18 and the National Science Foundation under Contract Nos. ECS021-8008 and ECS-0214867 is greatly acknowledged.

Appendix A

We are using pseudo-differential operators (PDO) here as a compact notation to write integral convolution operators. The general principle is that one has a function of two variables $A(x,z)$. One applies the PDO $A(x, \nabla_x)$ to a function $V(x)$ by:

- Replacing ∇_x by $i\xi$. Here ξ is the frequency variable corresponding to x in the Fourier transform.
- Multiplying $A(x, i\xi)$ with the Fourier transform $V(\xi)$.
- Back Fourier transforming.

This means to perform the following operations:

$$A(x, \nabla_x)V(x) = \int A(x, i\xi)V(\xi)e^{i\xi \cdot x} d\xi, \quad V(\xi) = (2\pi)^{-d} \int V(y)e^{-i\xi \cdot y} dy .$$

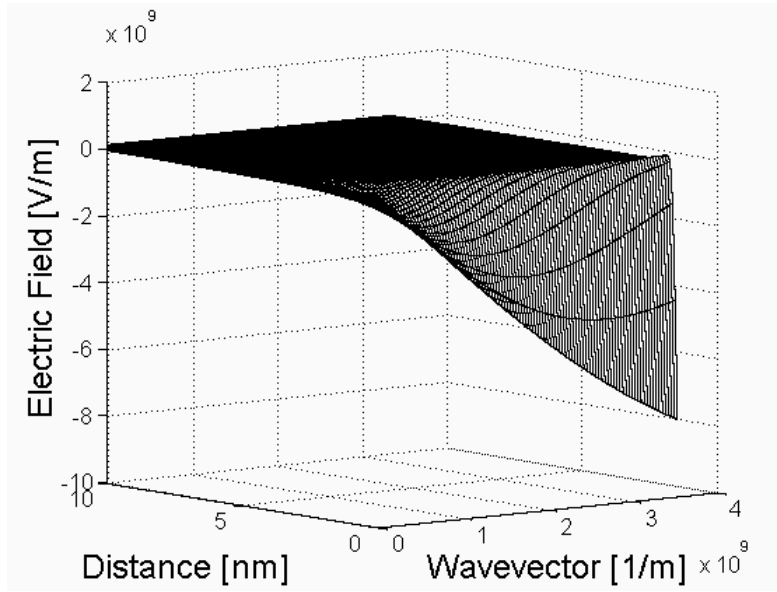
In the above expression, d is the dimension of x , i.e. $d = 1$ or $d = 2$ in our case.

Figure Captions

- Figure 1. The variation of the quantum barrier field with depth and wavevector k . Top panel: low energy electrons, bottom panel: high energy electrons.
- Figure 2. Variation of the sheet electron density versus gate voltage in a MOS capacitor structure.
- Figure 3. Electron localization within the triangular potential barrier for the case when quantization effects are not included in the model (top panel) and for the case when we include quantum-mechanical space-quantization effects by using the effective potential approach presented in this paper (bottom panel).
- Figure 4. Electron distribution in the device without (left panel) and with (right panel) the incorporation of quantum-mechanical size-quantization effects.
- Figure 5. Variation of the sheet electron density along the channel. **New-barr** corresponds to the case when we only include the influence of the barrier field. **New** represents the case when we include both the barrier and the Hartree contributions to the total electric field.
- Figure 6. Average electron velocity (top panel) and average electron energy (bottom panel) variation along the channel.
- Figure 7. Device transfer characteristic for $V_D = 0.1$ V.
- Figure 8. Device output characteristics.

Figure 1. Ahmed et al.

Low-energy electrons.



High-energy electrons.

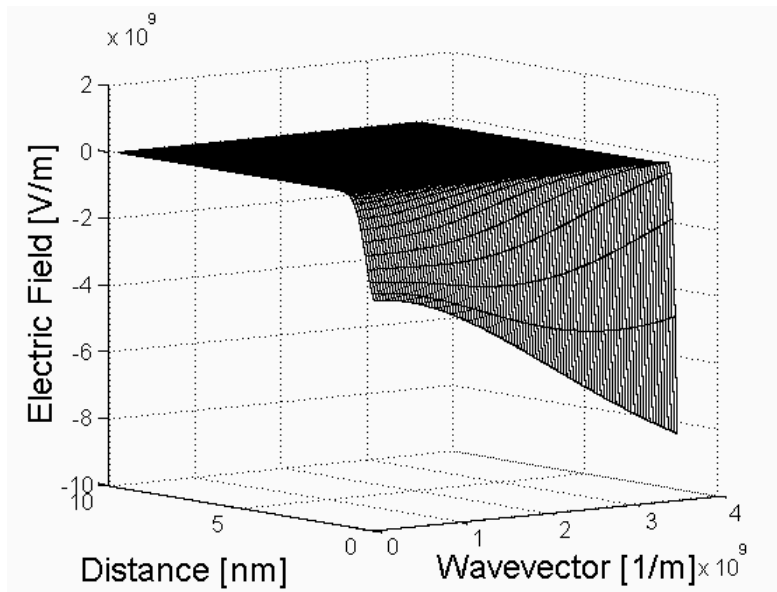


Figure 2. Ahmed et al.

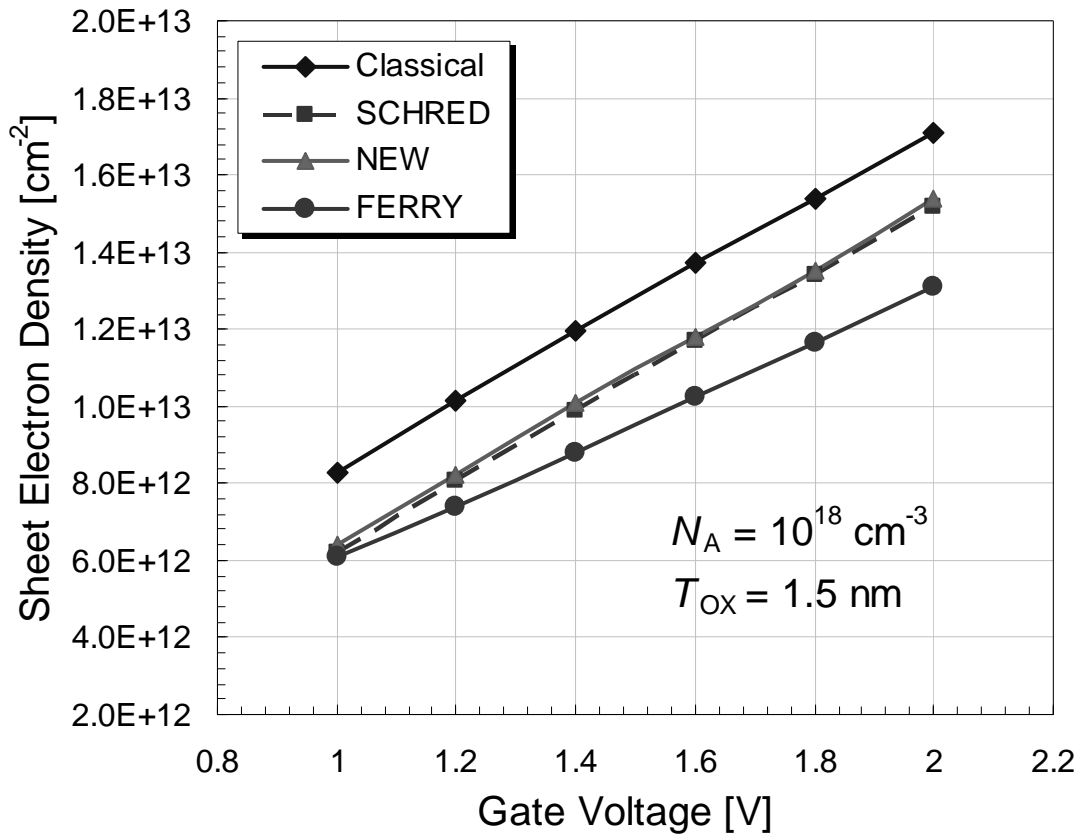


Figure 3. Ahmed et al.

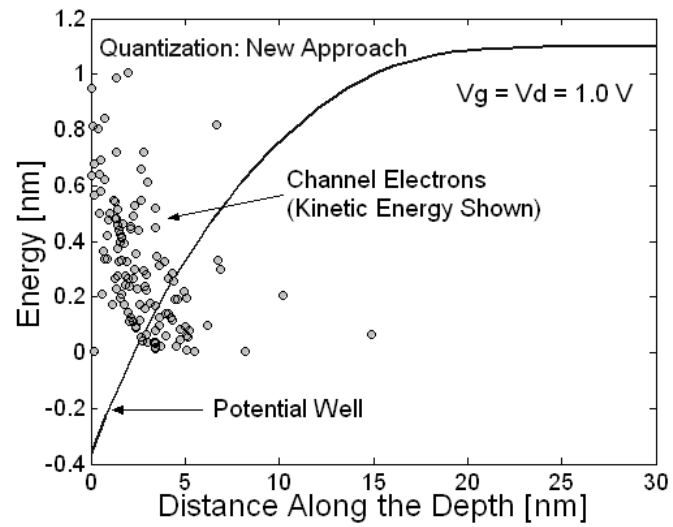
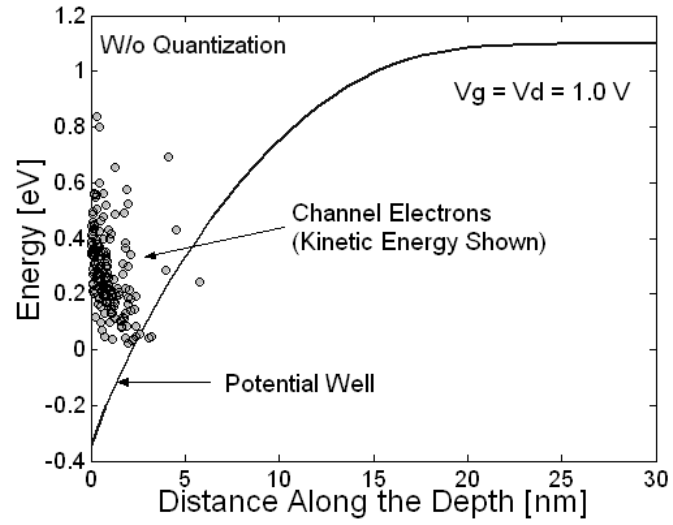


Figure 4. *Vasileska et al.*

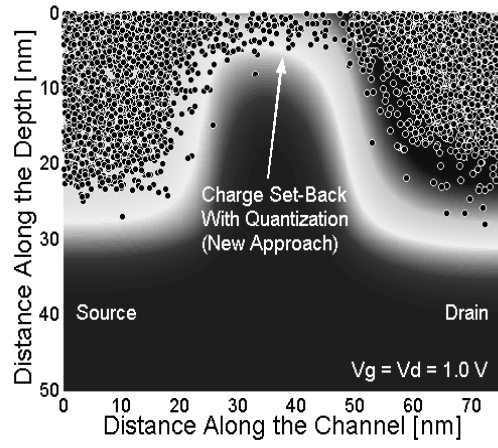
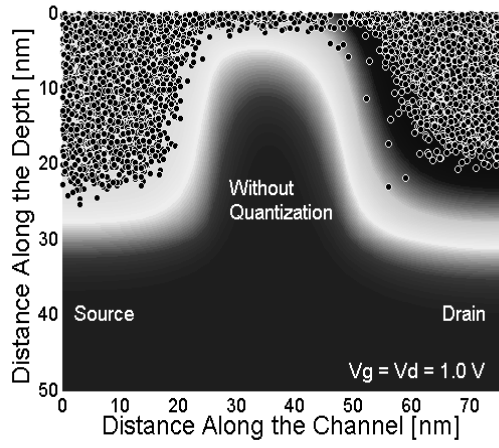


Figure 5. Ahmed et al.

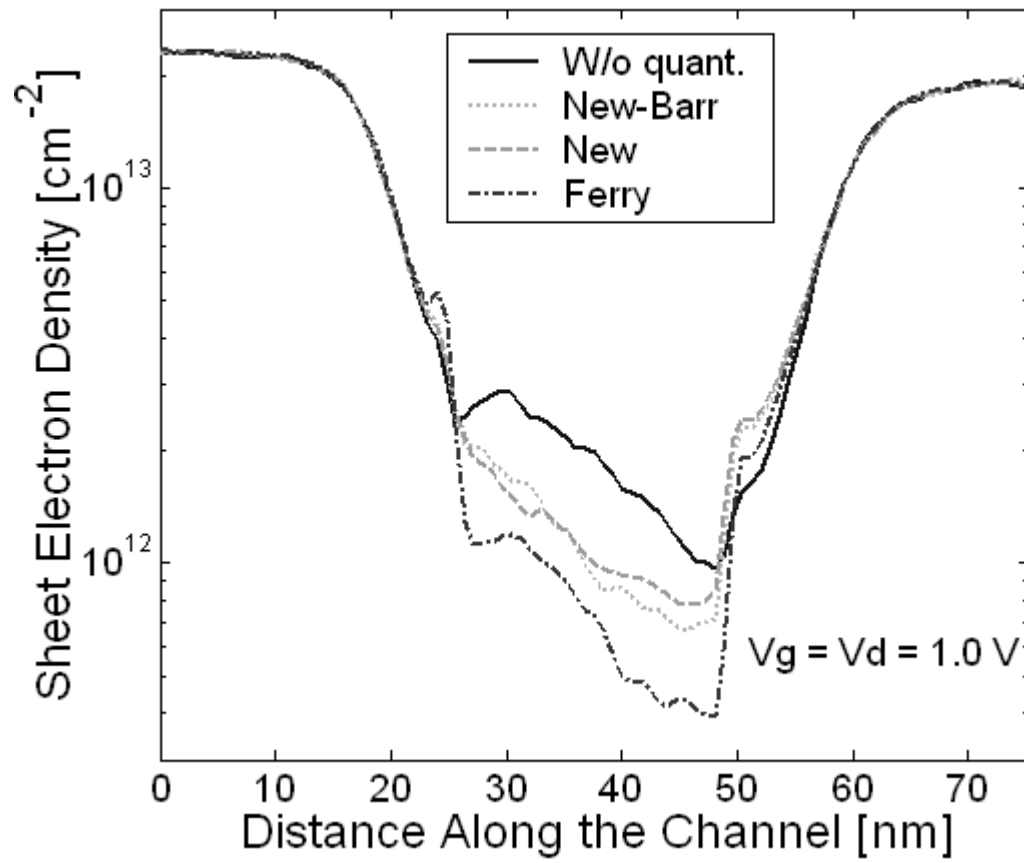


Figure 6. Ahmed et al.

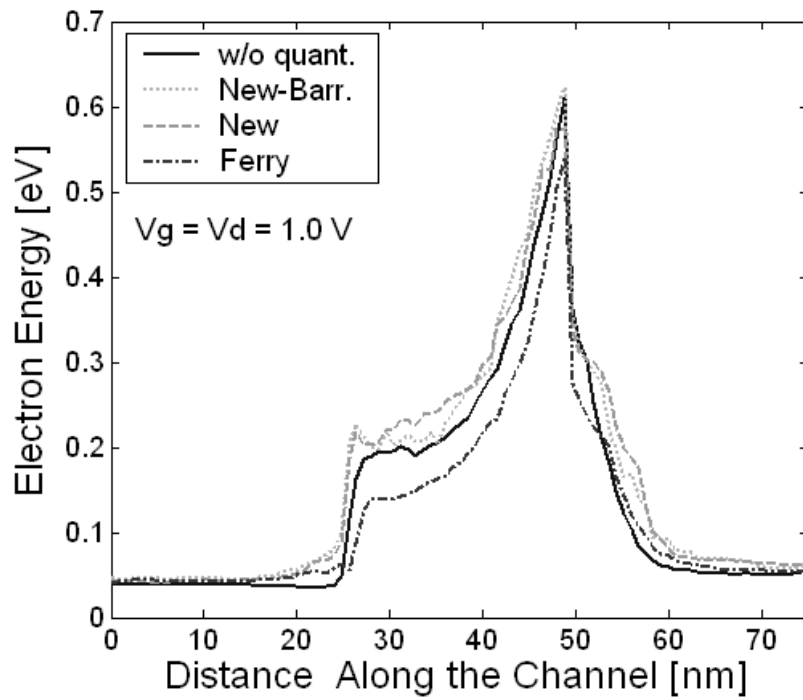
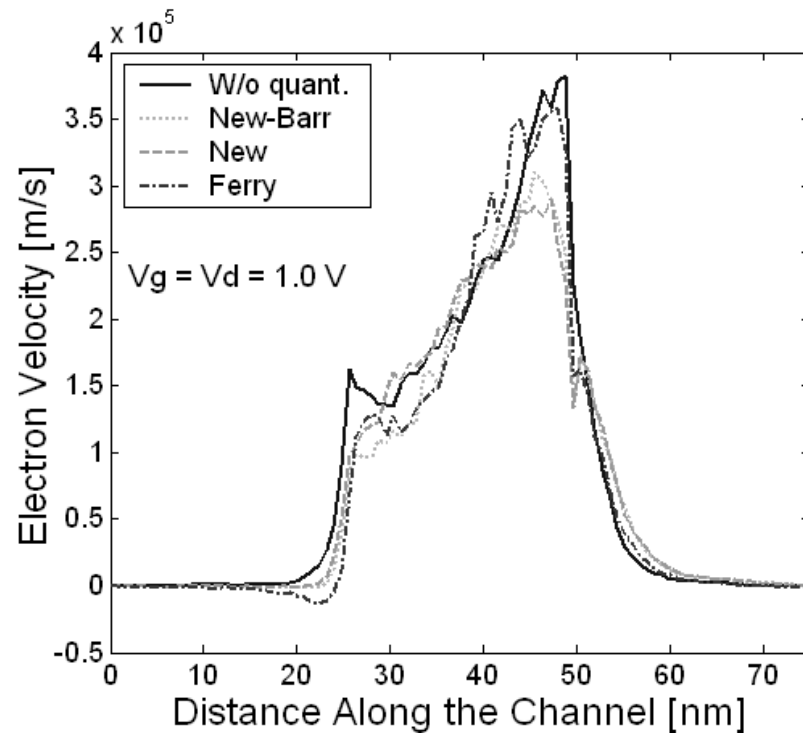


Figure 7. Ahmed et al.

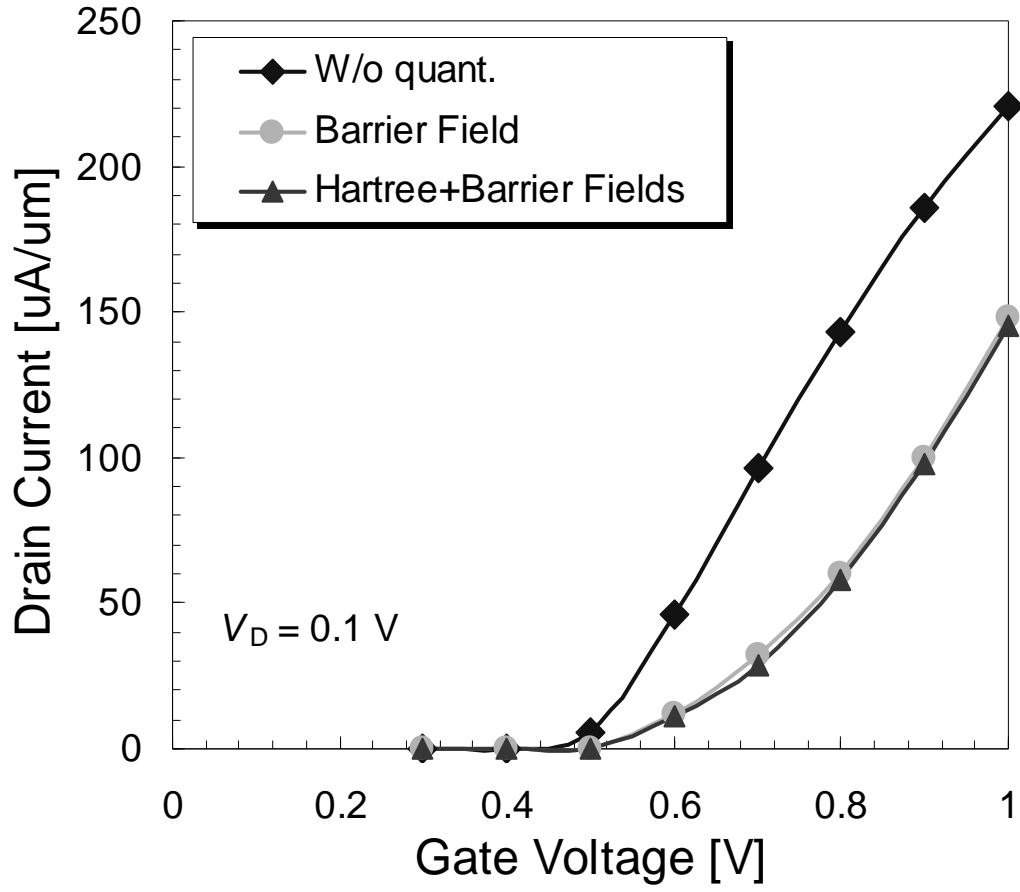
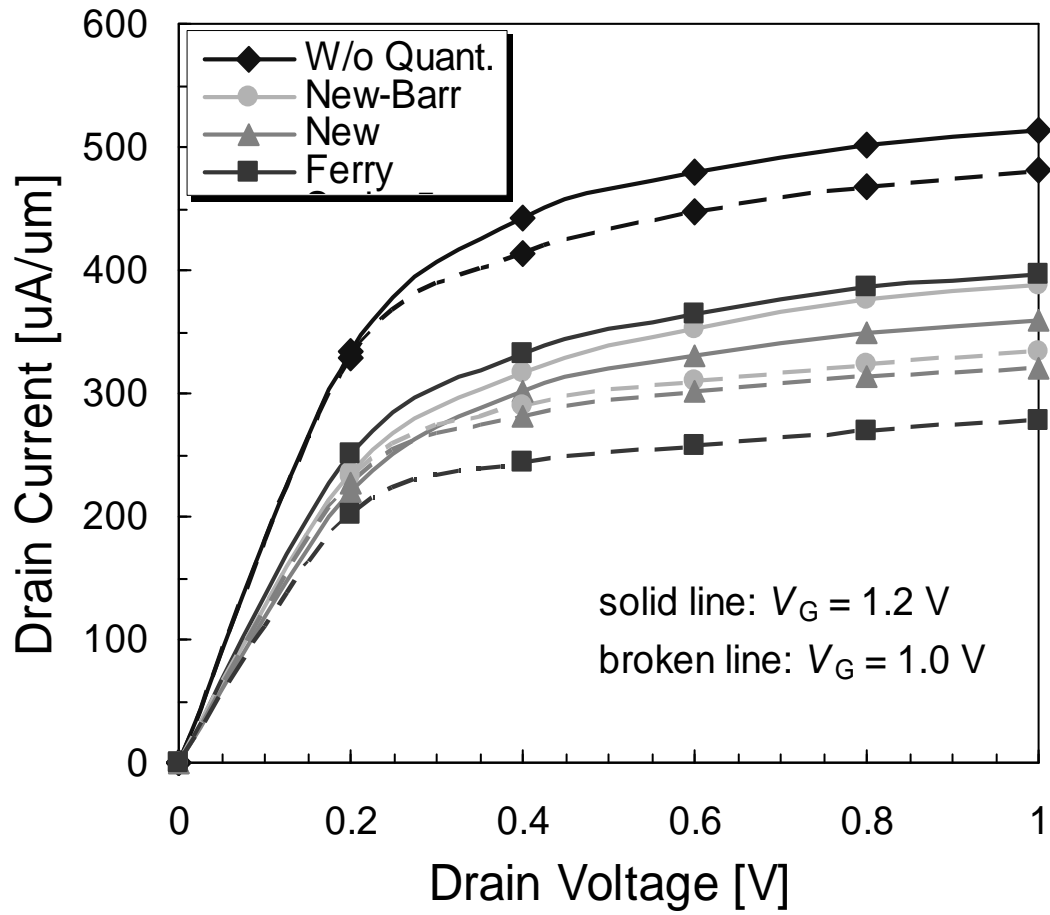


Figure 8. Ahmed et al.



References

- [1] L. de Broglie, "Sur la possibilité de relier les phénomènes d'interférence et de diffraction à la théorie des quanta de lumière", *C. R. Acad. Sci. Paris*, Vol. 183, pp. 447-448, 1926.
- [2] L. de Broglie, "La structure atomique de la matière et du rayonnement et la Mécanique ondulatoire", *C. R. Acad. Sci. Paris*, Vol. 184, pp. 273-274, 1927.
- [3] E. Madelung, "Quantentheorie in hydrodynamischer form", *Z. Phys.*, Vol. 40, pp. 322-326, 1926.
- [4] D. Bohm, "A suggested interpretation of the quantum theory in terms of hidden variables. I.", *Phys. Rev.*, Vol. 85, pp. 166-179, 1952.
- [5] D. Bohm, "A suggested interpretation of the quantum theory in terms of hidden variables. II", *Phys. Rev.*, Vol. 85, pp. 180-193, 1952.
- [6] C. Dewdney and B. J. Hiley, "A quantum potential description of one-dimensional time-dependent scattering from square barriers and square wells", *Found. Phys.*, Vol. 12, pp. 27-48, 1982.
- [7] G. J. Iafrate, H. L. Grubin, and D. K. Ferry, "Utilization of quantum distribution functions for ultra-submicron device transport", *Journal de Physique*, Vol. 42 (Colloq. 7), pp. 307-312, 1981.
- [8] E. Wigner, "On the quantum correction for thermodynamic equilibrium", *Phys. Rev.*, Vol. 40, pp. 749-759, 1932.
- [9] D. K. Ferry and J.-R. Zhou, "Form of the quantum potential for use in hydrodynamic equations for semiconductor device modeling", *Phys. Rev. B*, Vol. 48, pp. 7944-7950, 1993.
- [10] P. Feynman and H. Kleinert, "Effective classical partition functions", *Phys. Rev. A*, Vol. 34, pp. 5080-5084, 1986.
- [11] C. L. Gardner and C. Ringhofer, "Smooth quantum potential for the hydrodynamic model", *Phys. Rev. E*, Vol. 53, pp. 157-167, 1996.
- [12] C. Ringhofer and C. L. Gardner, "Smooth QHD model simulation of the resonant tunneling diodes", *VLSI Design*, Vol. 8, pp. 143-146, 1998.
- [13] C. Ringhofer, C. Gardner and D. Vasileska, "Effective potentials and quantum fluid models: A thermodynamic approach", *Inter. J. on High Speed Electronics and Systems* 13, 771, 2003.